ROTOR POWER LOSS MEASUREMENTS FOR HETEROPOLAR AND HOMOPOLAR MAGNETIC BEARINGS

P. E. Allaire
M. E. F. Kasarda
E. H. Maslen
G. R. Gillies

Mechanical, Aerospace, and Nuclear Engineering
University of Virginia, Charlottesville, VA 22901, USA
Tel: 804-924-6209 Fax: 804-982-2037 E-mail: pea@virgina.edu

ABSTRACT

The rotor losses in three magnetic bearing configurations were evaluated by measuring the rundown speed of the rotor, in air, after it was spun up to speeds of approximately 30,000 rpm. The kinetic energy of the rotor is converted to power loss (heat) during the run down.

Magnetic bearing power losses were measured in three different bearings. The effects of bias flux density, air gap thickness and flux path design were studied.

INTRODUCTION

Rotor losses in magnetic bearings are very important for many applications. In some applications such as aircraft gas turbines, space devices, or energy storage flywheels, these losses must be minimized to maximize the length of time the rotating machine can operate on a fixed energy or power supply. In other applications such as large compressors or electric motors, the heating caused by the magnetic bearing must be removed and excessive heating can be a major problem.

While not extensive, some power loss studies have been published in the open literature. Matsumura, et al [1] discussed magnetic bearing losses including a partial Fourier analysis of magnetic flux as seen by the rotor as it passes the poles in the bearing. Higuchi, et al. [2] presented some experimental rotating loss data in magnetic bearings. Ueyama and Fujimoto [3] gave power loss results in an eight pole radial bearing. Matsumura and Hatake [5] discussed a Fourier analysis of fringing and leakage effects on eddy current losses, indicating that pole edge effects may be the most important consideration. Kasarda et al. [5,6] conducted loss measurements in a low speed test rig, operating up to approximately 2800 rpm (DN = 175,000), in air.

Kasarda, et al. [7] discussed the design of the present high speed test rig in some detail and gave a sensitivity analysis of the loss modeling based upon the theoretical parameters involved. Kasarda, et al. [8] presented high speed loss results, using the same test rig employed for the work in this paper, for an 8 pole radial bearing constructed of silicon iron laminated materials. The rotor operated at a top speed of about 32,000 rpm, corresponding to a $\bar{D}N$ value of 2.9×10^6 mm rpm. Variations in pole winding configuration and bias flux were examined. Bias flux was found to be very significant while pole winding was found to be not very significant. An analytical /empirical model was then applied to the loss measurements by Kasarda, et al. [9].

TEST RIG

The test rig consists of a shaft with two magnetic bearings and two induction motors located at the shaft ends, as shown in Fig. 1. It has been designed to measure the power losses in magnetic bearings by accurately measuring the conversion

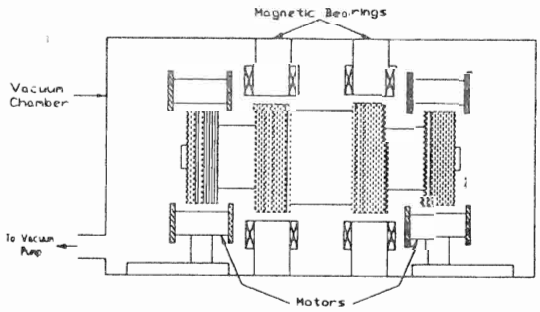

Figure 1. Diagram of Magnetic Bearing Loss Test Rig

of the rotor's kinetic energy into heat. This is done by measuring the time it takes for the rotor to run down from one speed to another. The rotor kinetic energy due to rotation is

$$E_k = \frac{1}{2} J\omega^2 \qquad (1)$$

The power loss is the time derivative of the kinetic energy

$$P_k = \frac{dE_k}{dt} = J\omega\frac{d\omega}{dt} + \frac{\omega^2}{2}\frac{dJ}{dt} \qquad (2)$$

The second term is small for this test because the rotor does not have large dimensional changes so this expression reduces to

$$P_k = J\omega\frac{d\omega}{dt} = P_e + P_h + P_w \qquad (3)$$

The polar moment of inertia of the rotor, J, is easily determined from a calculation and $\omega(t)$ is easily measured from the rundown tests. On the right hand side of this equation, the power loss is written as the sum of the power loss due to eddy currents, P_e, the power loss due to hysteresis, P_h, and the power loss due to windage, P_w. It has been shown in previous work [7,8,9] that the power loss can be written in terms of frequency dependent parameters as

$$P_k = C_h\omega + C_e\omega^2 + C_w\omega^{2.8} \qquad (4)$$

based upon analytical/empirical models. Here, the skin effects are small and are neglected [8].

The test rig has been designed so that the only significant loss mechanisms come from the magnetic bearings: eddy current losses, hysteresis losses, and air drag. The two electric motors drive the rotor up to peak operating speed and then they are shut off. The motor stators have been shown to not have any significant residual magnetic drag during run down [8].

A vacuum chamber will be employed in future work to eliminate air drag but that feature was not in place for the work reported here. No thrust bearings are present in the test rig: the rotor is centered by reluctance forces in the radial bearings. Thus there are no thrust bearing losses.

Fig. 2 shows a rotor assembly drawing. The outer diameter of the bearing journals is 91.4 mm (3.6 in) and the test rig is designed to operate up to 50,000 rpm resulting in a DN of 4.5×10^6 mm-rpm. The

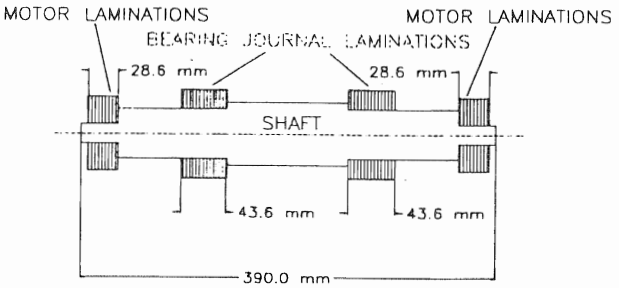

Figure 2. Rotor Assembly Drawing

rotor first critical speed is at approximately 84,000 rpm so the rotor is considered rigid. Fig. 3 shows a full assembly drawing of the test rig.

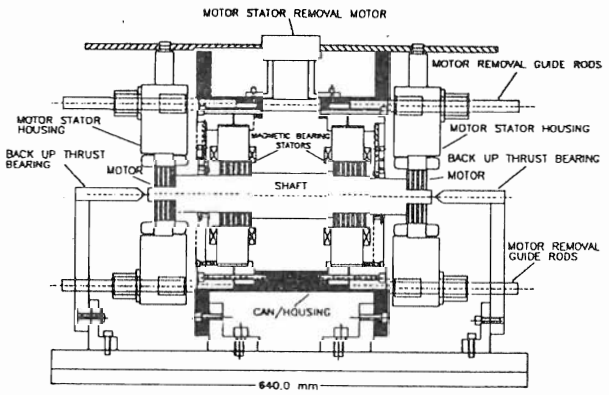

Figure 3. Full Test Rig Assembly Drawing

MAGNETIC BEARING STATOR PROPERTIES

Two comparable bearing stators have been tested for losses: Stator S1: an 8 pole radial planar (heteropolar) bearing and Stator S2: an 2-plane, 8 pole homopolar

bearing. Both of these stators have equal total pole face areas, with the stator surface area is 6,748 mm^2 (10.46 in^2) for one bearing. The axial pole length of the homopolar stator is one half of the heteropolar but there are two poles. The stators were constructed of 0.356 mm (0.014 in) 3% silicon iron laminations. The number of edges that the journal passes is the same for both bearings. Both stators have the same ID.

MAGNETIC BEARING ROTOR PROPERTIES

Three laminated rotors with bearing journals were employed. All are constructed of 3% silicon iron lamination thickness of 0.356 mm (0.014 in). They are approximately 91.4 mm (3.6 in) OD with slight differences to obtain the clearances desired. The laminations are stacked axially along the shaft to restrict the development of eddy currents moving in the axial direction. The three rotors have two different air gaps, Rotor R1 has a nominal air gap of 0.762 mm (0.030 in) while rotors R2 and R3 have a nominal air gap of 0.381 mm (0.015 in). The difference between rotors R2 and R3 is that rotor R3 is somewhat longer to accommodate the extra length of the homopolar stator (S2).

HETEROPOLAR BEARINGS

The heteropolar bearing geometry is shown in Fig. 4. It has 8 poles, rotor OD = 91.4 mm (3.60 in), shaft OD = 50.8 mm (2.0 in), stator OD = 196.2 mm (7.726 in), axial length of bearing L = 43.6 mm (1.715 in)

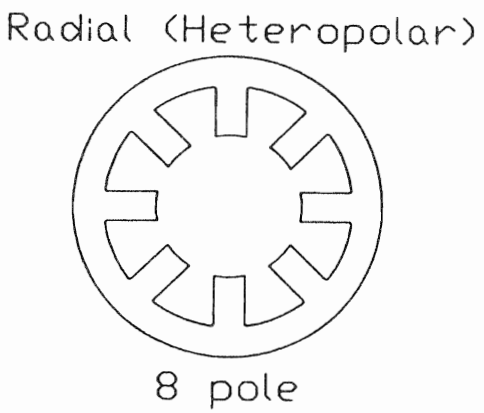

Figure 4. Heteropolar Bearing Geometry

(without coils). The radial length of each leg is 31.8 mm (1.253 in) and the circumferential width of each leg is 21.1 mm (0.79 in). The relative permeability of the rotor and stator material is estimated at 3,000. Two air gaps were run for this bearing, rotor R1: g_1 = 0.762 mm (0.030 in) and rotor R2: g_2 = 0.381 mm (0.015 in). The different gap thicknesses were obtained by using two different rotors with different rotor lamination OD. Table 1 shows the heteropolar and homopolar bearing configurations.

Table 1. Heteropolar and Homopolar Bearing Configurations

Bearing	Stator	Rotor
No. 1 (Heteropolar)	S1	R1
No. 2 (Heteropolar)	S1	R2
No. 3 (Homopolar)	S2	R3

Fig. 5 shows the measured power loss data for the heteropolar bearing with the two different air gaps at three different values of bias flux density, 0.4 Tesla, 0.5 Tesla, and 0.6 Tesla. Rundown plots are not shown for all of these cases but the method of reducing the data is discussed later in the paper and some example rundown plots are shown later, in Fig. 8.

DATA REDUCTION

Rundown data was evaluated to determine power loss using the following model

$$\frac{d\omega}{dt} = b_1 + b_2\omega + b_3\omega^{1.8} \qquad (5)$$

where the coefficients are defined as

$$b_1 = \frac{C_h}{J} \; ; \; b_2 = \frac{C_e}{J} \; ; \; b_3 = \frac{C_w}{J} \qquad (6)$$

from (3) and (4). An analytical

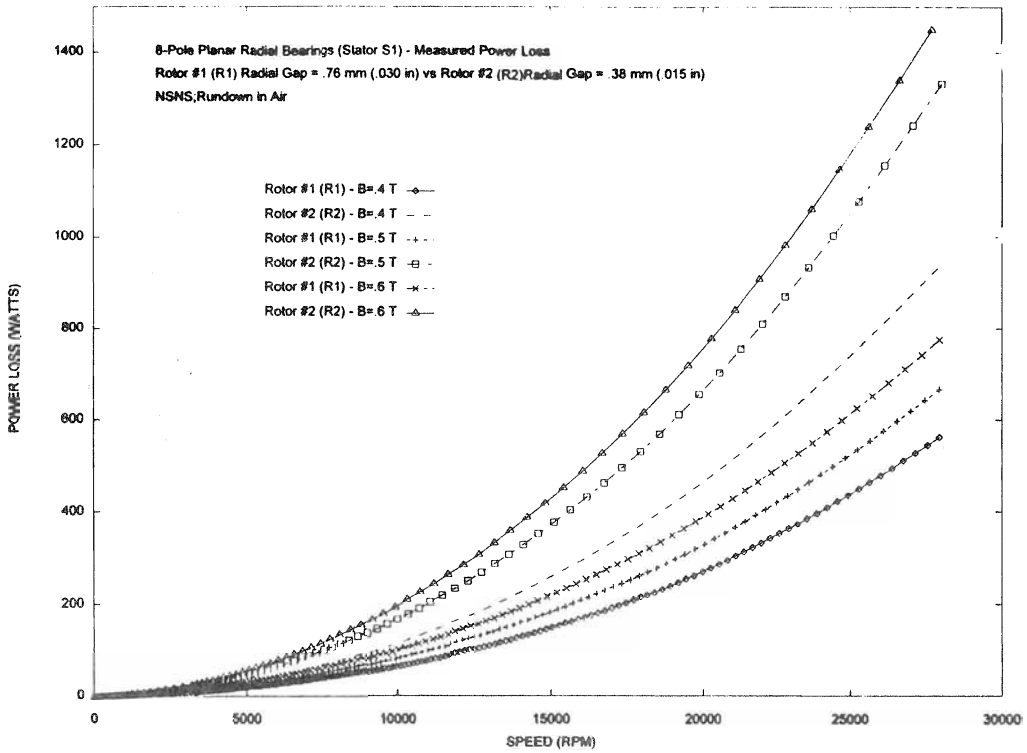

Figure 5. Measured Magnetic Bearing Power Loss vs. Speed at Three Bias Flux Density Values for Two Air Gap Thicknesses.

Table 2. Power Loss Coefficients For Magnetic Bearing Data Presented in Fig. 5 For Three Bias Flux Density Values and Two Air Gap Thicknesses.

	B = .4 T		B = .5 T		B=.6 T	
	Bearing #1 (Gap = .76mm)	Bearing #2 (Gap = .38mm)	Bearing #1 (Gap = .76mm)	Bearing #2 (Gap = .38mm)	Bearing #1 (Gap = .76mm)	Bearing #2 (Gap = .38mm)
Hysteresis (rpm-s^{-1})	b_1= -17.6	b_1= -16.0	b_1= -22.1	b_1= -22.2	b_1= -26.8	b_1= -25.2
Eddy Current (s^{-1})	b_2= -4.6×10^{-3}	b_2= -1.0×10^{-2}	b_2= -6.2×10^{-3}	b_2= -1.6×10^{-2}	b_2= -7.9×10^{-3}	b_2= -1.9×10^{-2}
Windage (rpm$^{-.8}$-s^{-1})	b_3= -8.6×10^{-7}	b_3= -7.4×10^{-7}	b_3= -7.8×10^{-7}	b_3= -8.2×10^{-7}	b_3= -7.1×10^{-7}	b_3= -4.0×10^{-7}

expression for the actual speed curve was determined for each case and minimized using a simplex search method [8]. The measured power loss was then determined from (4) and (6). The coefficients b_1, b_2 and b_3 are given in Table 2 for the data in Fig. 5. The hysteresis coefficients are nearly the same for both bearings at a given value of flux density indicating that the hysteresis effects are nearly the same for each bearing. The eddy current coefficients are much larger, by a factor of 2 to 3, for the case with the smaller gap of 0.381 mm (0.015 in). Thus the eddy currents are the major difference in the larger losses at lower gap thickness (or lower tip clearance ratio). The windage coefficients are nearly the same for the two bearings when the bias flux density is the same. There is a difference at the bias flux density of 0.6 Tesla for the small gap configuration which may indicate that skin effects are becoming important.

HOMOPOLAR BEARING

A 2-plane, 8 pole homopolar bearing was tested. Figure 7 shows the geometry of the bearing. The stator, S2, was constructed of 0.356 mm (0.014 in) 3% silicon iron laminations. The rotor, R3, has 3% silicon iron laminations thickness of 0.356 mm (0.014 in), The air gap thickness was 0.381 mm (0.015 in) for the homopolar bearing.

Rundown data was taken for the

homopolar bearing operating in the same speed range as the heteropolar bearing. Figure 8 shows a plot of the rundown data for both the heteropolar bearing No. 2 and the

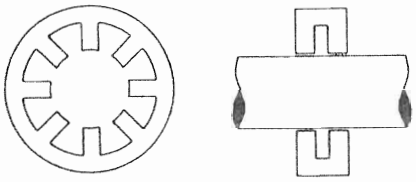

Figure 7. Homopolar Bearing Geometry

homopolar bearing No. 3 at a bias flux density of 0.3 Tesla. The speed range is up to 30,000 rpm. The air gap thickness and flux density is the same for both bearings so the curves clearly indicates the lower loss performance of the homopolar design.

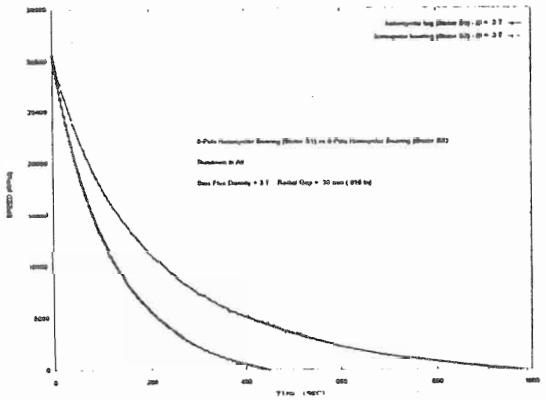

Figure 8. Rundown Speed vs. Time For Heteropolar and Homopolar Bearings at 0.3 Tesla Bias Flux

This data was converted to power loss data and the results plotted in Fig. 9. The power loss values were

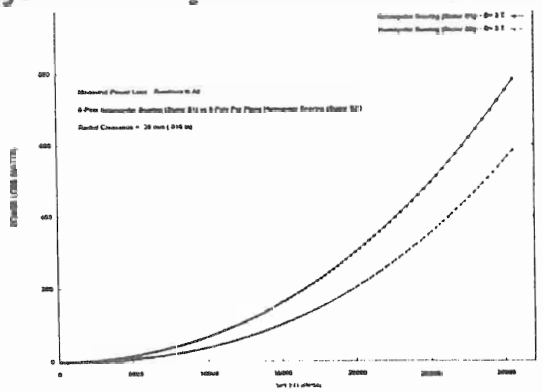

Figure 9. Measured Power Loss vs. Speed For Heteropolar and Homopolar Bearings at 0.3 Tesla Bias Flux

converted into loss coefficients as given in Table 3 from (5) and (6). The hysteresis coefficient, b_1, is lower for the homopolar bearing. This is to be expected as rotating hysteresis losses should be lower in the homopolar bearing. The eddy current coefficient, b_2, is also significantly lower. The windage coefficient is approximately the

Table 3. Power Loss Coefficients For Magnetic Bearing Data Presented in Fig. 9 For Heteropolar and Homopolar Bearing

	B = .3 T	
	Heteropolar Coefficients	Homopolar Coefficients
Hysteresis ($rpm \cdot s^{-1}$)	$b_1 = -10.4$	$b_1 = -4.3$
Eddy Current (s^{-1})	$b_2 = -5.3 \times 10^{-3}$	$b_2 = -1.9 \times 10^{-3}$
Windage ($rpm^{-1} \cdot s^{-1}$)	$b_3 = -1.0 \times 10^{-6}$	$b_3 = -1.1 \times 10^{-6}$

same indicating that the longer length rotor does not apparently develop much higher windage loss.

MAGNETIC FLUX DENSITY MEASUREMENTS

The magnetic flux density was measured in the air gaps for all cases. Example measured values are given in Table 4 for a bias flux density of 0.6 Tesla in the two 8 pole heteropolar bearings. The bias current in the bearing coils corresponding to the data in Table 4 was 1.94 amps. The difference in the air gaps is due to the load on the bearing and experimental variability on using the flux probe. The average value for both bearings is approximately 0.62 Tesla.

CONCLUSIONS

Magnetic bearing rotor power loss variation with speed, bias flux density, air gap thickness, and flux path design were studied. The variation of rotor power loss vs. speed was evaluated for three different bearings. In each case, the total power loss varied approximately with ω^2 over the entire operating range tested.

As a general rule, the influence of the bias flux density seems to approximately proportional B^2, at least for much of the data presented in this paper. This seems to be due to the strong role of eddy current effects at high rotational speeds. The B^2 law, as one might expect from transformer loss theory, is seen to

be valid for much of this data. Skin effects will be quantified in future work.

The air gap effect is significant. A reduction in air gap by a factor of 2 yields an approximate increase in power loss by a factor of 2. Thus the power loss is approximately inversely proportional to the air gap thickness. This will be made more quantitative in future work.

Table 4. Measured Air Gap Flux Levels in Bearings No. 1 and No. 2

Pole No.	Stator No.1 Flux Density (T)	Stator No. 2 Flux Density (T)
1	0.71	0.68
2	0.60	0.62
3	0.66	0.66
4	0.59	0.57
5	0.62	0.63
6	0.56	0.52
7	0.67	0.70
8	0.56	0.59

The homopolar bearing has significantly lower power losses than a comparable heteropolar bearing. For the bearings tested here, the heteropolar power loss was approximately 800 watts at 30,000 rpm as compared to approximately 600 watts for the homopolar bearing at the same speed. This is about a 25% reduction for the homopolar bearing. The reduction is due to both lower eddy currents and lower hysteresis losses. The windage losses are about the same.

REFERENCES

1. Matsumura, F., Fujita, M., and Ozaki, Y., 1988, "Characteristics of Friction on Magnetic Bearings," Trans. IEE of Japan, 108-D, No. 5, pp 462-468.

2. Higuchi, T., Mizuno, T., and Miyake, S., 1986, "Experimental Study of Rotational Loss in Magnetic Bearings," Proc. Conf. IPE, Japan, pp. 53-54.

3. Ueyama, H., and Fujimoto, Y., 1990, "Iron Losses and Windy Losses of Rotational Speed Rotor Suspended by Magnetic Bearings," Proceedings of 2nd International Symposium on Magnetic Bearings, Tokyo, Japan, pp. 237-242.

4. Matsumura, F., and Hatake, K., 1992, "Relation between Magnetic Pole Arrangement and Magnetic Loss in Magnetic Bearing," Proceedings of Third International Conference on Magnetic Bearings, Alexandria, Virginia, USA, pp. 274-283.

5. Kasarda, M.E., Allaire, P.E., Hope, R.W., and Humphris, R.R., 1993, "Measured and Predicted Losses in Planar Radial Magnetic Bearings," Proceedings of Mag '93, Alexandria, VA.

6. Kasarda, M.E., and Allaire, P.E., 1995, "Experimentally Measured and Improved Calculated Losses in Planar Radial Magnetic Bearings," Accepted for STLE Transactions, 1996.

7. Kasarda, M. E. F., Allaire, P. E., Maslen, E. H. and Gillies, G. T., 1994, "Design of a High Speed Rotating Loss Test Rig For Radial Magnetic Bearings," Proceedings, Fourth International Symposium on Magnetic Bearings, ETH Zurich.

8. Kasarda, M. E. F., Allaire, P. E., Maslen, E. H., Brown, G. R., and Gillies, G. T., "High Speed Rotor Losses in a Radial 8-Pole Magnetic Bearing, Part 1: Experimental Measurement," Paper 96-GT-470, International Gas Turbine Conference, Birmingham, England, June 1996.

9. Kasarda, M. E. F., Allaire, P. E., Maslen, E. H., Brown, G. R., and Gillies, G. T., "High Speed Rotor Losses in a Radial 8-Pole Magnetic Bearing, Part 2: Analytical/Empirical Models and Calculation," Paper 96-GT-471, International Gas Turbine Conference, Birmingham, England, June 1996.

ACKNOWLEDGEMENT

This work was supported in part by NASA Lewis Research Center with Dr. Gerald Brown as Project Monitor.